NUWC-NPT Technical Report 11,320
1 November 2001

An Inverse Method for Measuring the Flexural Wave Properties of a Beam

Andrew J. Hull
Field Team Operations Office

David A. Hurdis
Submarine Sonar Department

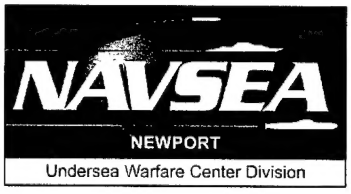

Naval Undersea Warfare Center Division
Newport, Rhode Island

PREFACE

The work described in this report was funded under Project No. F51041, "ELF Electromagnetic Noise Sources and Mitigation," principal investigator Grant Miller (Code 3411). The sponsoring activity is the Office of Naval Research, Dennis McGregor (Code 313).

The technical reviewer for this report was Bruce Sandman (Code 01).

The authors wish to thank Gerald Messina (Code 7014) for his assistance in setting up the experiment and collecting the data. Additionally, the authors express appreciation to Karen Holt (Code 543) for her help with the technical editing of the manuscript.

Reviewed and Approved: 1 November 2001

William H. Andresen
Director, Field Team Operations

REPORT DOCUMENTATION PAGE

Form Approved
OMB No. 0704-0188

1. AGENCY USE ONLY *(Leave blank)*	2. REPORT DATE	3. REPORT TYPE AND DATES COVERED
	1 November 2001	

4. TITLE AND SUBTITLE

An Inverse Method for Measuring the Flexural Wave Properties of a Beam

5. FUNDING NUMBERS

6. AUTHOR(S)

Andrew J. Hull
David A. Hurdis

7. PERFORMING ORGANIZATION NAME(S) AND ADDRESS(ES)

Naval Undersea Warfare Center Division
1176 Howell Street
Newport, RI 02841-1708

8. PERFORMING ORGANIZATION REPORT NUMBER

TR 11,320

9. SPONSORING/MONITORING AGENCY NAME(S) AND ADDRESS(ES)

Office of Naval Research
800 North Quincy St.
Arlington, VA 22217

10. SPONSORING/MONITORING AGENCY REPORT NUMBER

11. SUPPLEMENTARY NOTES

12a. DISTRIBUTION/AVAILABILITY STATEMENT

Approved for public release; distribution is unlimited.

12b. DISTRIBUTION CODE

13. ABSTRACT (Maximum 200 words)

This report derives an inverse method to measure the complex flexural wavenumber and wave propagation coefficients of a beam. The new approach obtains seven measured transfer functions by vibrating the beam transversely with any set of corresponding boundary conditions. These measurements are then combined to yield closed-form solutions of the beam parameters. The test method is subjected to a Monte Carlo simulation, which shows that it is relatively immune to external noise in the data, and to an experiment, which validates the technique when it is applied to actual laboratory data.

14. SUBJECT TERMS

Sonar Signal Processing; Wave Propagation; Beam Coefficients; Sonar Arrays; Flexural Wave Properties

15. NUMBER OF PAGES

36

16. PRICE CODE

17. SECURITY CLASSIFICATION OF REPORT	18. SECURITY CLASSIFICATION OF THIS PAGE	19. SECURITY CLASSIFICATION OF ABSTRACT	20. LIMITATION OF ABSTRACT
Unclassified	Unclassified	Unclassified	SAR

TABLE OF CONTENTS

Page

LIST OF ILLUSTRATIONS ii

LIST OF TABLES ii

INTRODUCTION 1

SYSTEM MODEL AND INVERSE SOLUTION 3

NUMERICAL SIMULATIONS 10

EXPERIMENT 14

CONCLUSIONS 22

REFERENCES 23

APPENDIX — CLOSED-FORM SOLUTION USED FOR THE NUMERICAL SIMULATIONS A-1

LIST OF ILLUSTRATIONS

Figure		Page
1	Estimated and Actual Values of Flexural Wavenumber Versus Frequency Using a 0.02 Noise Value	12
2	Flexural Wavenumber Estimation Error (θ) Versus Frequency for a Single Simulation Using a 0.02 Noise Value	14
3	Estimation of Flexural Wavenumber Versus Frequency for Experiment	16
4	Estimation of Coefficient *A* Versus Frequency for Experiment	17
5	Estimation of Coefficient *B* Versus Frequency for Experiment	18
6	Estimation of Coefficient *C* Versus Frequency for Experiment	19
7	Estimation of Coefficient *D* Versus Frequency for Experiment	20
8	Measured and Estimated Transfer Function Versus Frequency	21
A-1	Beam with Two Springs Attached to the Shaker Table	A-4

LIST OF TABLES

Table		Page
1	Transfer Function Error (e) Versus Estimation Error (ε)	13

AN INVERSE METHOD FOR MEASURING THE FLEXURAL WAVE PROPERTIES OF A BEAM

INTRODUCTION

Measuring the flexural wave properties of beams is important because these parameters significantly contribute to the static and dynamic response of structures. An effective approach for obtaining such measurements uses an "inverse" method that typically involves choosing a model of the system under study and fitting experimental data to the model by letting the unknown parameters be free variables.

One of the first researchers to examine what is called the inverse problem was Prony,[1] who developed a technique for estimating the parameters of damped sinusoids from evenly spaced measurements. Today, the "Prony methods," which describe the majority of equally spaced multisensor experimental techniques, are most notably used by Grosh and Williams,[2] who have developed a modified version to deconvolve the helical wave spectrum of a point-driven cylindrical shell using a simulated experiment. Their procedure first estimates the wavenumbers using a root-finding algorithm applied to a characteristic polynomial and then relies on the resulting values to find the wave propagation coefficients with a least-squares algorithm.

Another proponent of the inverse method was Ram,[3] whose technique when applied to a flexural beam uses eigenvalue and eigenvector data to build a model of a discretized system from which mass and stiffness parameters can be extracted. In addition, Linjama and Lahti,[4] Bauman,[5] and Mace and Halkyard[6] have estimated structural intensity and its corresponding properties (usually shear force, transverse velocity, bending moment, and angular velocity) in a beam. There is also an inverse technique described by Koss and Karczub[7] that uses the wave propagation coefficients to estimate the strain field in a beam; however, it does not solve explicitly for the flexural wavenumber. In still another study, McDaniel et al.[8] show how transient loading provides a means to estimate frequency-dependent damping, as well as investigate the transfer of data from the spatial domain into the wavenumber domain. Finally,

McDaniel and Shepard[9] have proposed a solution to the inverse problem that is based on the use of unevenly spaced measurements and an iterative method to determine flexural wavenumber.

In the study presented in this report, an inverse method is developed to measure the complex flexural wavenumber and the corresponding wave propagation coefficients of a beam that is undergoing transverse motion. Based on the transformation of experimental measurements to parameter estimates, the technique results in a closed-form solution. The approach is typically used for measuring the flexural wave properties of cars, ships, aircraft, bridges, buildings, and other common structures that contain beams.

More specifically, the inverse technique described here combines seven transfer function measurements to yield closed-form values of flexural wavenumber and wave propagation coefficients at any given test frequency. Numerical simulations are presented to show that the method is relatively immune to noise in measurement data. An experiment is also conducted on a beam, during which the method is applied to the data to yield the flexural wavenumber and the wave propagation coefficients of an actual system. When the estimated transfer function is calculated from these estimated parameters and compared to the original measured data, it is found that the parameter estimation method is extremely accurate.

It should be noted that the inverse process can easily incorporate beam parameter perturbations, making it an ideal method for design alteration testing. If the beam material properties change, the method is simply rerun using the original experimental setup with the new beam. Because the process is independent of boundary conditions, it is not necessary to duplicate the beam-mounting conditions, which is especially useful when the rotational and translational compliance of the mount may change from experiment to experiment. Furthermore, the inverse method is independent of beam length, allowing comparisons of beams of varying length. Finally, the calculations needed to compute flexural wavenumber parameters can be done in seconds, which permits real-time evaluations of beam properties.

SYSTEM MODEL AND INVERSE SOLUTION

The system model of the transverse motion of the beam is the Bernoulli-Euler beam equation, written as

$$EI\frac{\partial^4 u(x,t)}{\partial x^4} + \rho A_b \frac{\partial^2 u(x,t)}{\partial t^2} = 0 \ , \tag{1}$$

where x is the distance along the length of the beam (m), t is time (s), u is the displacement of the beam in the (transverse) y-direction (m), E is the (complex) Young's modulus ($\mathrm{N/m^2}$), I is the moment of inertia ($\mathrm{m^4}$), ρ is the density ($\mathrm{kg/m^3}$), and A_b is the cross-sectional area of the beam ($\mathrm{m^2}$). Implicit in equation (1) is the assumption that plane sections remain plane during bending (or transverse motion). Additionally, Young's modulus, the moment of inertia, the density, and the cross-sectional area remain constant along the entire length of the beam. The displacement is modeled as a steady-state response in time and is expressed as

$$u(x,t) = U(x,\omega)\exp(\mathrm{i}\omega t) \ , \tag{2}$$

where ω is the frequency of excitation (rad/s), $U(x,\omega)$ is the temporal Fourier transform of the transverse displacement, and i is the square root of -1. The temporal solution to equation (1), derived using equation (2) and written in terms of trigonometric functions, is

$$\begin{aligned} U(x,\omega) = {} & A(\omega)\cos[\alpha(\omega)x] + B(\omega)\sin[\alpha(\omega)x] \\ & + C(\omega)\cosh[\alpha(\omega)x] + D(\omega)\sinh[\alpha(\omega)x] \ , \end{aligned} \tag{3}$$

where $A(\omega)$, $B(\omega)$, $C(\omega)$, and $D(\omega)$ are wave propagation coefficients and $\alpha(\omega)$ is the flexural wavenumber given by

$$\alpha(\omega) = \left[\frac{\omega^2}{(EI/\rho A_b)}\right]^{1/4} \ . \tag{4}$$

For brevity, the ω dependence is omitted from the wave propagation coefficients and the flexural wavenumber throughout the remainder of the report. Note also that equations (3) and (4) are independent of boundary conditions and that the inverse model developed here does not require boundary condition specifications or assumptions.

Equation (3) has five unknowns and is nonlinear with respect to the unknown flexural wavenumber. It will be shown that the use of seven independent, equally spaced measurements allows the five unknowns to be estimated with closed-form solutions. To begin, seven frequency-domain transfer functions of acceleration (or displacement) are measured at some location and are then divided by a common reference measurement. Each transfer function is collected by two accelerometers placed at different locations on the beam (one may be placed at the base of the shaker table). The seven measurements are set equal to the theoretical expression given in equation (3). Without loss of generality, the middle measurement location corresponds to $x = 0$. (This location does not necessarily have to be placed at the middle of the beam.) The seven equations are written as

$$T_{-3} = \frac{U_{-3}(-3\delta,\omega)}{V_0(\omega)} = A\cos(3\alpha\delta) - B\sin(3\alpha\delta) + C\cosh(3\alpha\delta) - D\sinh(3\alpha\delta) \ , \tag{5}$$

$$T_{-2} = \frac{U_{-2}(-2\delta,\omega)}{V_0(\omega)} = A\cos(2\alpha\delta) - B\sin(2\alpha\delta) + C\cosh(2\alpha\delta) - D\sinh(2\alpha\delta) \ , \tag{6}$$

$$T_{-1} = \frac{U_{-1}(-\delta,\omega)}{V_0(\omega)} = A\cos(\alpha\delta) - B\sin(\alpha\delta) + C\cosh(\alpha\delta) - D\sinh(\alpha\delta) \ , \tag{7}$$

$$T_0 = \frac{U_0(0,\omega)}{V_0(\omega)} = A + C \ , \tag{8}$$

$$T_1 = \frac{U_1(\delta,\omega)}{V_0(\omega)} = A\cos(\alpha\delta) + B\sin(\alpha\delta) + C\cosh(\alpha\delta) + D\sinh(\alpha\delta) \ , \tag{9}$$

$$T_2 = \frac{U_2(2\delta,\omega)}{V_0(\omega)} = A\cos(2\alpha\delta) + B\sin(2\alpha\delta) + C\cosh(2\alpha\delta) + D\sinh(2\alpha\delta)\ , \tag{10}$$

and

$$T_3 = \frac{U_3(3\delta,\omega)}{V_0(\omega)} = A\cos(3\alpha\delta) + B\sin(3\alpha\delta) + C\cosh(3\alpha\delta) + D\sinh(3\alpha\delta)\ , \tag{11}$$

where δ is the sensor-to-sensor separation distance (m) and $V_0(\omega)$ is the reference measurement. Note that the transfer functions given in equations (5)–(11) are dimensionless.

Equation (7) is added to equation (9) and equation (6) is added to equation (10), yielding

$$A\cos(\alpha\delta) + C\cosh(\alpha\delta) = \frac{T_1 + T_{-1}}{2} \tag{12}$$

and

$$A\cos(2\alpha\delta) + C\cosh(2\alpha\delta) = \frac{T_2 + T_{-2}}{2}\ . \tag{13}$$

Equations (8), (12), and (13) are combined and manipulated using multiple-angle regular and hyperbolic trigonometric expressions to produce

$$\cosh(\alpha\delta)\cos(\alpha\delta) + \left\{\left(\frac{T_1 + T_{-1}}{2T_0}\right)\left[\cosh(\alpha\delta) + \cos(\alpha\delta)\right]\right\} + \left(\frac{T_2 + T_{-2} + 2T_0}{4T_0}\right) = 0\ . \tag{14}$$

It is noted at this point that a zero-finding algorithm applied to equation (14) is sufficient to solve for the unknown flexural wavenumber. However, a closed-form solution of the flexural wavenumber is preferred, so further mathematical manipulation is required. Thus, equation (7) is subtracted from equation (9), equation (6) is subtracted from equation (10), and equation (5) is subtracted from equation (11), resulting in

$$B\sin(\alpha\delta)+D\sinh(\alpha\delta)=\frac{T_1-T_{-1}}{2}\ , \tag{15}$$

$$B\sin(2\alpha\delta)+D\sinh(2\alpha\delta)=\frac{T_2-T_{-2}}{2}\ , \tag{16}$$

and

$$B\sin(3\alpha\delta)+D\sinh(3\alpha\delta)=\frac{T_3-T_{-3}}{2}\ , \tag{17}$$

respectively. Equations (15), (16), and (17) are combined and manipulated using multiple-angle regular and hyperbolic trigonometric expressions to give

$$\cosh(\alpha\delta)\cos(\alpha\delta)+\left\{\left[\frac{T_2-T_{-2}}{2(T_1-T_{-1})}\right][\cosh(\alpha\delta)+\cos(\alpha\delta)]\right\}+\left[\frac{T_3-T_{-3}+T_1-T_{-1}}{4(T_1-T_{-1})}\right]=0\ . \tag{18}$$

Combining equations (14) and (18) now results in a binomial expression with respect to the cosine function, which is written as

$$a\cos^2(\alpha\delta)+b\cos(\alpha\delta)+c=0\ , \tag{19}$$

where

$$a=4T_1^2-4T_{-1}^2+4T_{-2}T_0-4T_0T_2\ , \tag{20}$$

$$b=2T_{-2}T_{-1}-2T_{-2}T_1+2T_{-1}T_0-2T_0T_1+2T_{-1}T_2-2T_1T_2+2T_0T_3-2T_{-3}T_0\ , \tag{21}$$

and

$$c = T_{-1}^2 - T_1^2 + T_2^2 - T_{-2}^2 + T_{-3}T_{-1} - T_{-1}T_3 + T_{-3}T_1 - T_1T_3 + 2T_0T_2 - 2T_{-2}T_0 \ . \qquad (22)$$

Equation (19) is now solved using

$$\cos(\alpha\delta) = \frac{-b \pm \sqrt{b^2 - 4ac}}{2a} = \phi \ , \qquad (23)$$

where ϕ is typically a complex number. Based on the sign in front of the radical, equation (23) contains two solutions to equation (19). Only one solution, however, will have an absolute value less than unity as required by the cosine function, and it is this root that is further manipulated. The inversion of equation (23) allows the complex-valued flexural wavenumber α to be solved as a function of ϕ at every frequency in which a measurement is made. The solution to the real part of α is

$$\mathrm{Re}(\alpha) = \begin{cases} \dfrac{1}{2\delta}\mathrm{Arc}\cos(s) + \dfrac{n\pi}{2\delta} & n \text{ even} \\ \dfrac{1}{2\delta}\mathrm{Arc}\cos(-s) + \dfrac{n\pi}{2\delta} & n \text{ odd} \end{cases} , \qquad (24)$$

where

$$s = [\mathrm{Re}(\phi)]^2 + [\mathrm{Im}(\phi)]^2 - \sqrt{\left\{[\mathrm{Re}(\phi)]^2 + [\mathrm{Im}(\phi)]^2\right\}^2 - \left\{2[\mathrm{Re}(\phi)]^2 - 2[\mathrm{Im}(\phi)]^2 - 1\right\}} \ , \qquad (25)$$

n is a non-negative integer, and the capital A denotes the principal value of the inverse cosine function. The value of n is determined from the function s, which is a periodically varying cosine function with respect to frequency. That is, while n is 0 at zero frequency, it increases by 1 every time s cycles through π radians (180°). It is noted here that increasing the integer n allows the estimation process to be used beyond the Nyquist spacing criteria of the sensors because n keeps a count of the number of aliasing cycles between the sensors and thus accounts

for these cycles in the measurement process. After the solution to the real part of α is found, the solution to the imaginary part of α is written as

$$\mathrm{Im}(\alpha) = \frac{1}{\delta}\log_e\left\{\frac{\mathrm{Re}(\phi)}{\cos[\mathrm{Re}(\alpha)\delta]} - \frac{\mathrm{Im}(\phi)}{\sin[\mathrm{Re}(\alpha)\delta]}\right\}. \tag{26}$$

The real and imaginary parts of α from equations (24) and (26), respectively, are combined to yield the complex flexural wavenumber.

Although normally considered less important than the estimate of the flexural wavenumber, the wave propagation coefficients are next determined with either an exact or ordinary least-squares solution. The exact solution is found by combining equations (12) and (13), which results in

$$A = \frac{2T_0\cosh(\alpha\delta) - (T_1 + T_{-1})}{2[\cosh(\alpha\delta) - \cos(\alpha\delta)]} \tag{27}$$

and

$$C = \frac{(T_1 + T_{-1}) - 2T_0\cos(\alpha\delta)}{2[\cosh(\alpha\delta) - \cos(\alpha\delta)]}. \tag{28}$$

Combining equations (15) and (16) yields

$$B = \frac{2(T_1 - T_{-1})\cosh(\alpha\delta) - (T_2 - T_{-2})}{4\sin(\alpha\delta)[\cosh(\alpha\delta) - \cos(\alpha\delta)]} \tag{29}$$

and

$$D = \frac{(T_2 - T_{-2}) - 2(T_1 - T_{-1})\cos(\alpha\delta)}{4\sinh(\alpha\delta)[\cosh(\alpha\delta) - \cos(\alpha\delta)]}. \tag{30}$$

Equations (27)–(30) thus represent the exact estimates of the complex wave propagation coefficients.

When the second method is used to estimate these coefficients, an ordinary least-squares fit is applied to all the data points.[2, 6, 7] This approach begins with a formulation of the problem that uses N (= 7) algebraic equations, where N is the number of sensors. Written in matrix form, the expressions are

$$\mathbf{Ax} = \mathbf{b} \ , \tag{31}$$

where

$$\mathbf{A} = \begin{bmatrix} \cos(3\alpha\delta) & -\sin(3\alpha\delta) & \cosh(3\alpha\delta) & -\sinh(3\alpha\delta) \\ \cos(2\alpha\delta) & -\sin(2\alpha\delta) & \cosh(2\alpha\delta) & -\sinh(2\alpha\delta) \\ \cos(\alpha\delta) & -\sin(\alpha\delta) & \cosh(\alpha\delta) & -\sinh(\alpha\delta) \\ 1 & 0 & 1 & 0 \\ \cos(\alpha\delta) & \sin(\alpha\delta) & \cosh(\alpha\delta) & \sinh(\alpha\delta) \\ \cos(2\alpha\delta) & \sin(2\alpha\delta) & \cosh(2\alpha\delta) & \sinh(2\alpha\delta) \\ \cos(3\alpha\delta) & \sin(3\alpha\delta) & \cosh(3\alpha\delta) & \sinh(3\alpha\delta) \end{bmatrix}, \tag{32}$$

$$\mathbf{x} = \begin{bmatrix} A \\ B \\ C \\ D \end{bmatrix}, \tag{33}$$

and

$$\mathbf{b} = \begin{bmatrix} T_{-3} \\ T_{-2} \\ T_{-1} \\ T_0 \\ T_1 \\ T_2 \\ T_3 \end{bmatrix}. \tag{34}$$

The solution to equation (31) is

$$\mathbf{x} = (\mathbf{A}^{\mathrm{H}}\mathbf{A})^{-1}\mathbf{A}^{\mathrm{H}}\mathbf{b} \ , \tag{35}$$

where the superscript H denotes the complex conjugate transpose of the matrix. The least-squares method (equations (31)–(35)) is normally considered to be more accurate than the exact solution shown in equations (27)–(30) and is therefore used for the calculations in the remainder of the report. This increase in accuracy occurs because all seven data points are used to estimate the wave propagation coefficients rather than only the five data points used for the exact solution. It is noted that the above procedure for estimating flexural wavenumber and wave propagation coefficients from the data provides a series of closed-form equations.

NUMERICAL SIMULATIONS

The inverse method is first examined with numerical simulations that have varying amounts of noise added to the transfer functions. The configuration corresponding to the numerical simulations is shown in the appendix, along with the closed-form solution to the wave propagation coefficients for the specific boundary conditions of the beam.

First, a baseline problem is defined that uses a rectangular beam with the following physical properties: $E = 10^{11}(1+0.05\mathrm{i})$ N/m^2, $\rho = 5000$ kg/m^3, $A_b = 0.015$ m^2, $I = 2.81 \times 10^{-5}$ m^4, $L = 4$ m, $\delta = 0.5$ m, $k_1 = 2.5 \times 10^{10}$ N/m, and $k_2 = 5 \times 10^{10}$ N/m. To study the effects of errors, random numbers are added to the transfer functions according to the equation

$$T_e(\omega) = T(\omega) + e\{\mathrm{Re}[T(\omega)]\sigma_a + \mathrm{iIm}[T(\omega)]\sigma_b\} \ , \tag{36}$$

where e is the amount of error added to the transfer function and σ_a and σ_b are random numbers with zero mean and a variance of one. The value e is also called the noise value as it represents the amount of noise added to the transfer function (or *additive noise*).

Figure 1 is a plot of the estimated and actual values of flexural wavenumber α versus frequency using an error value of $e = 0.02$. The actual values (no noise) of the real part of α are shown as a solid line, and the estimated values (with noise) of the real part of α are depicted with x's in the upper plot. The actual values of the imaginary part of α are shown as a solid line, and the estimated values of the imaginary part of α are depicted with o's in the lower plot.

The effect of measurement error on the accuracy of the calculation of flexural wavenumber and wave propagation coefficients can be studied with Monte Carlo simulations. Eleven different values of e were used to build the transfer functions and then calculate the flexural wavenumber and wave propagation values. Estimation error at each frequency was defined with the equation

$$\theta(\omega_m) = \frac{\left\| \gamma_a(\omega_m) \right| - \left| \gamma_e(\omega_m) \right\|}{\max\left[\gamma_a(\omega_m), \gamma_e(\omega_m) \right]} , \tag{37}$$

where γ is either flexural wavenumber α or one of the wave propagation coefficients A, B, C, or D; $\theta(\omega_m)$ is the estimation error at the mth frequency; the subscript a corresponds to the actual (noiseless) value; and the subscript e corresponds to the estimated (calculated) value. Once this value is known, it can be summed across M frequencies using

$$\beta_j = \frac{1}{M} \sum_{m=1}^{M} \theta(\omega_m) , \tag{38}$$

where β_j is the average error for the jth Monte Carlo simulation. Finally, all the simulations can be summed using

$$\varepsilon = \frac{1}{J} \sum_{j=1}^{J} \beta_j , \tag{39}$$

where ε is the estimation error using J simulations.

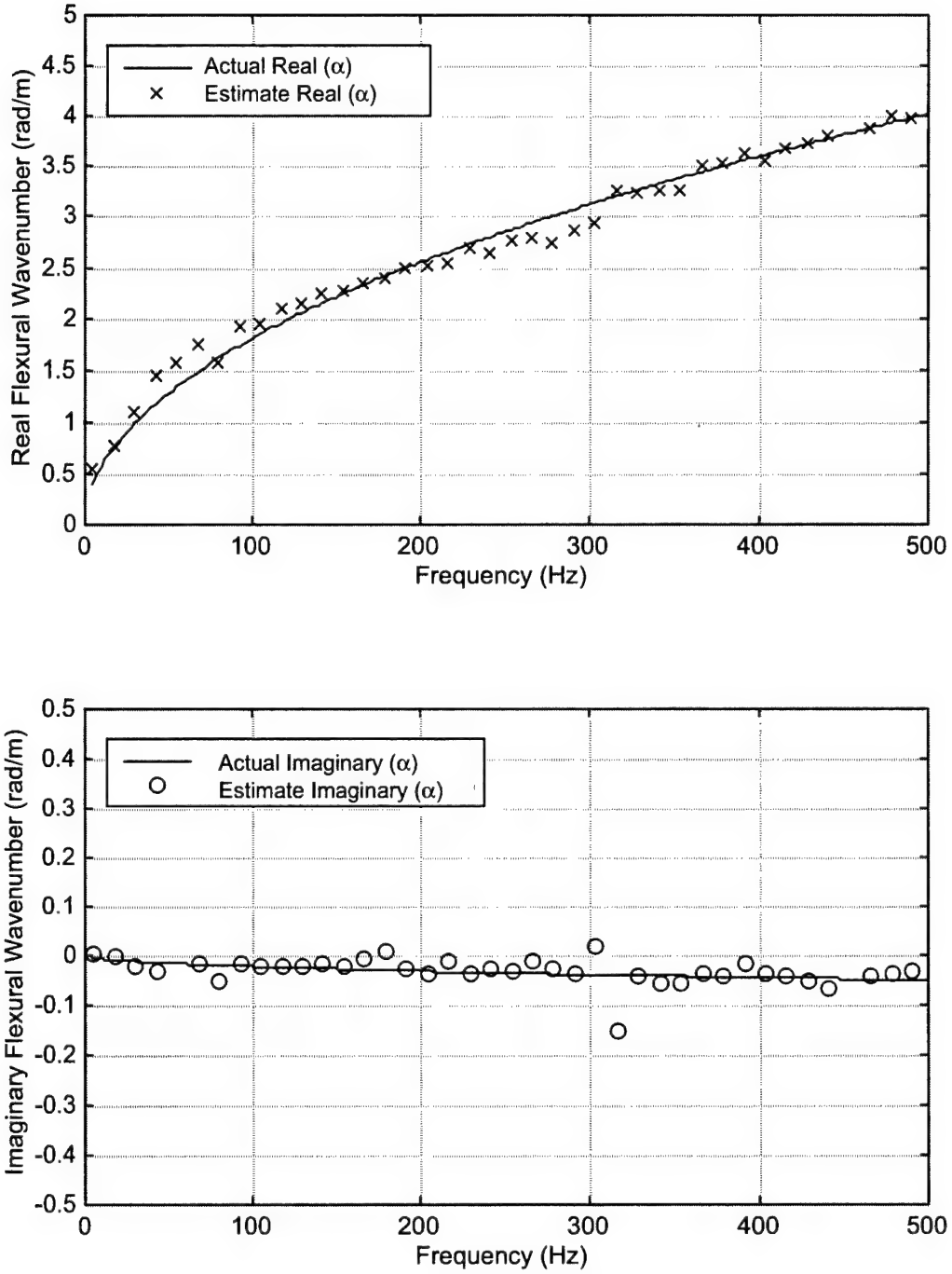

Figure 1. Estimated and Actual Values of Flexural Wavenumber Versus Frequency Using a 0.02 Noise Value

Table 1 provides a list of transfer function error (e) versus estimation error (ε). The frequency range of the values used to make this table is between 5 and 500 Hz, with the number of frequencies (M) used to calculate the estimation error being 200 and the number of simulations (J) for each value of e being 50. Errors less than 0.0001 are recorded as 0.

Table 1. Transfer Function Error (e) Versus Estimation Error (ε)

Transfer Function Error (e)	**Estimation Error (ε) for α**	**Estimation Error (ε) for A**	**Estimation Error (ε) for B**	**Estimation Error (ε) for C**	**Estimation Error (ε) for D**
0	0	0	0	0	0
0.005	0.048	0	0.0013	0.0009	0.0043
0.010	0.049	0	0.0021	0.0010	0.0046
0.015	0.050	0	0.0023	0.0014	0.0046
0.020	0.051	0	0.0027	0.0015	0.0048
0.025	0.051	0	0.0026	0.0016	0.0049
0.030	0.052	0	0.0031	0.0022	0.0049
0.035	0.054	0.0002	0.0033	0.0021	0.0049
0.040	0.055	0.0002	0.0037	0.0022	0.0049
0.045	0.057	0.0002	0.0038	0.0023	0.0049
0.050	0.059	0.0001	0.0039	0.0024	0.0049

Figure 2 shows a plot of flexural wavenumber estimation error (θ) versus frequency for a single simulation ($J = 1$) using a known transfer function error of $e = 0.02$. This numerical error analysis demonstrates that the process produces a very small error in the estimation of flexural wavenumber. Note that the larger estimation errors tend to occur near the lower frequency values.

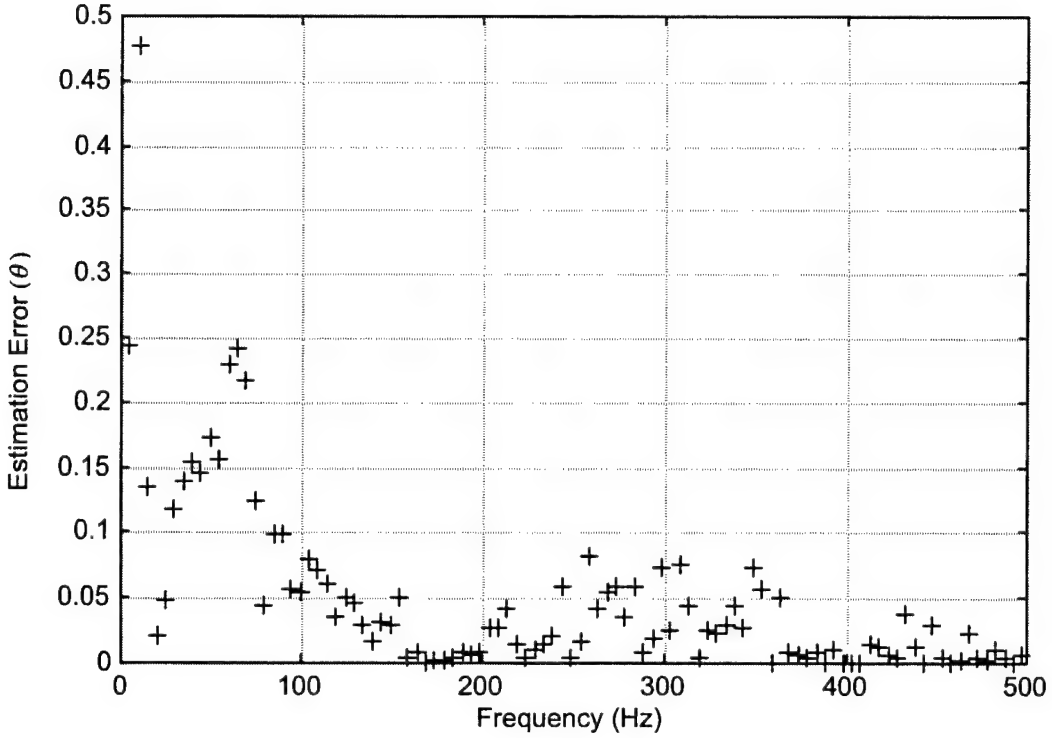

Figure 2. Flexural Wavenumber Estimation Error (θ) Versus Frequency for a Single Simulation Using a 0.02 Noise Value

EXPERIMENT

An experiment was conducted to test the validity of the inverse method when it was applied to actual laboratory data. A rectangular aluminum beam with the following properties was mounted to a shaker table using rigid aluminum mounts at each end: $A_b = 0.0077\ \text{m}^2$, $I = 6.66 \times 10^{-6}\ \text{m}^4$, $L = 1.07$ m, and $\delta = 0.133$ m.

It is important to note that this type of mounting system will not correspond to a translational spring boundary condition but rather to a combination of translational and rotational spring boundary conditions that are acting together at each end of the beam. Because the inverse method is independent of boundary conditions, this type of unknown and mixed boundary condition will not adversely impact the measurement process.

During the measurement process, nine equally spaced accelerometers were attached to the beam. The first accelerometer served as the reference measurement to the middle seven accelerometers, which correspond to equations (5)–(11). The ninth accelerometer was unused. Data taken in the time domain and transferred into the frequency domain using a Fourier transform were collected by the accelerometers from 4 to 400 Hz in swept-sine mode.

Figure 3 is a plot of the modeled and estimated values of flexural wavenumber α versus frequency. The modeled values of the real part of α are depicted with a solid line, and the estimated values are shown as x's in the upper plot. The modeled values of the imaginary part of α are depicted with a solid line, and the estimated values are shown as o's in the lower plot. The modeled values were determined by assuming that the aluminum bar had a Young's modulus of $7.31 \times 10^{10} (1 + 0.03i)$ N/m^2 and a density of 2700 kg/m^3 and then calculating the (modeled) wavenumber with equation (4). It is noted that at low frequency there is some disagreement between the model and the estimate, which has been well explained by McDaniel and Shepard.[9]

Figures 4–7, which show plots of the estimated wave propagation coefficients A, B, C, and D versus frequency, respectively, are calculated using the least-squares fit from equations (31)-(35). In all four figures, the upper plot is the magnitude and the lower plot is the phase angle.

In the final analysis, the method compares the measured data with the model, which is constructed using the estimated parameters. Figure 8 depicts the measurement and the model versus frequency at the sixth sensor ($x = 2\delta$), with the upper plot showing magnitude and the lower plot showing phase angle. It should be noted that the almost exact agreement between the measurement and the model is expected because the estimated parameters are based entirely on the measured data.

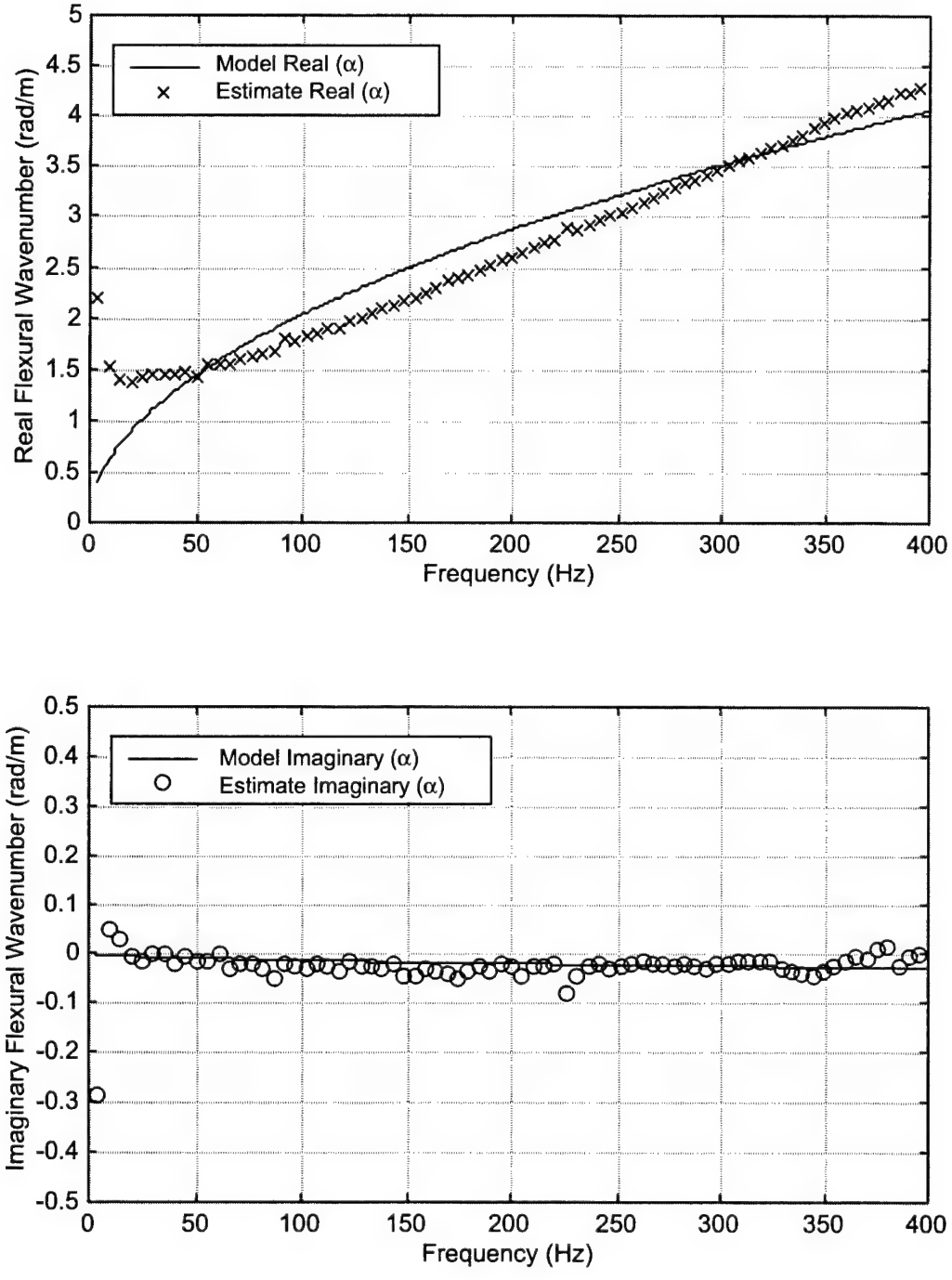

Figure 3. Estimation of Flexural Wavenumber Versus Frequency for Experiment

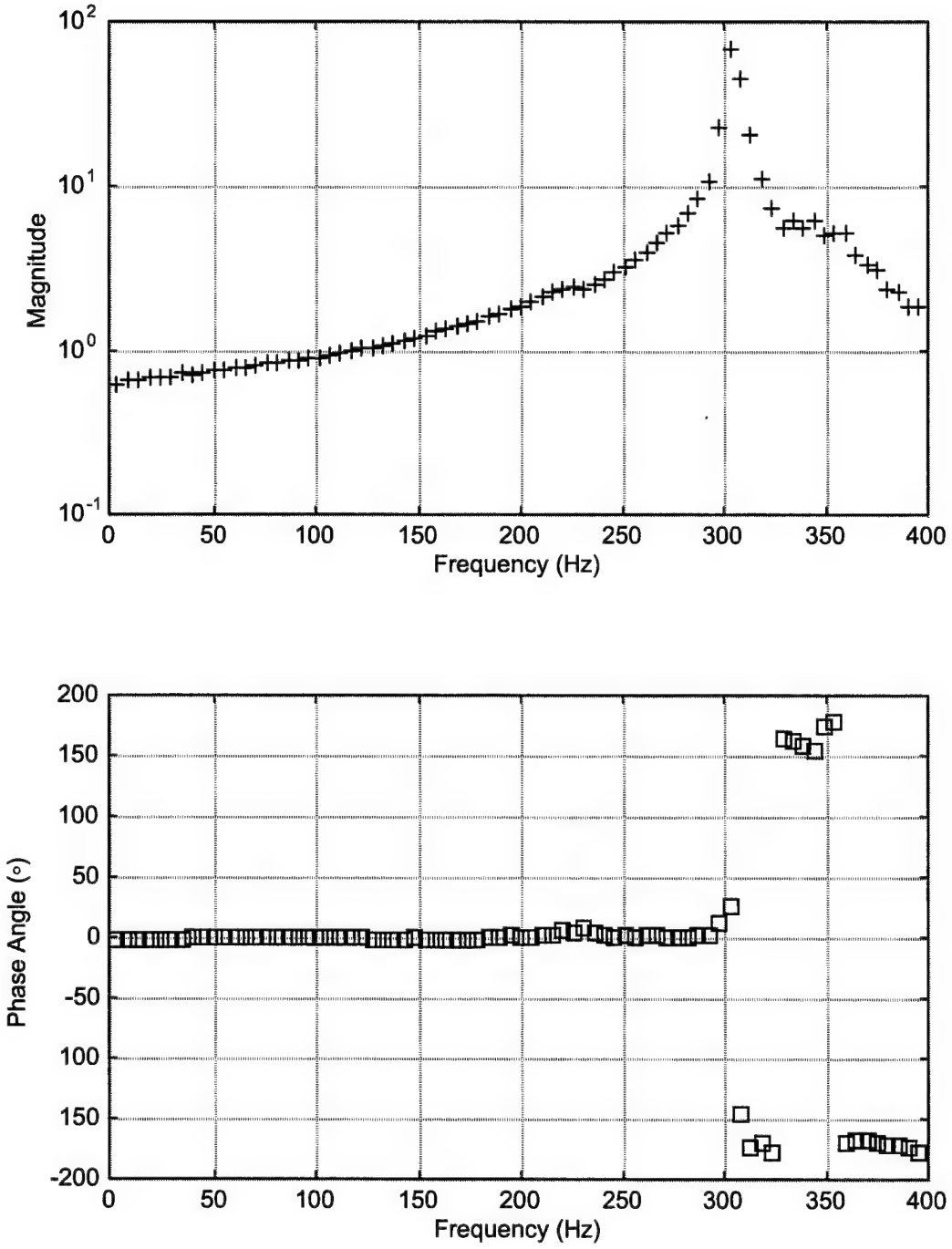

Figure 4. Estimation of Coefficient A Versus Frequency for Experiment

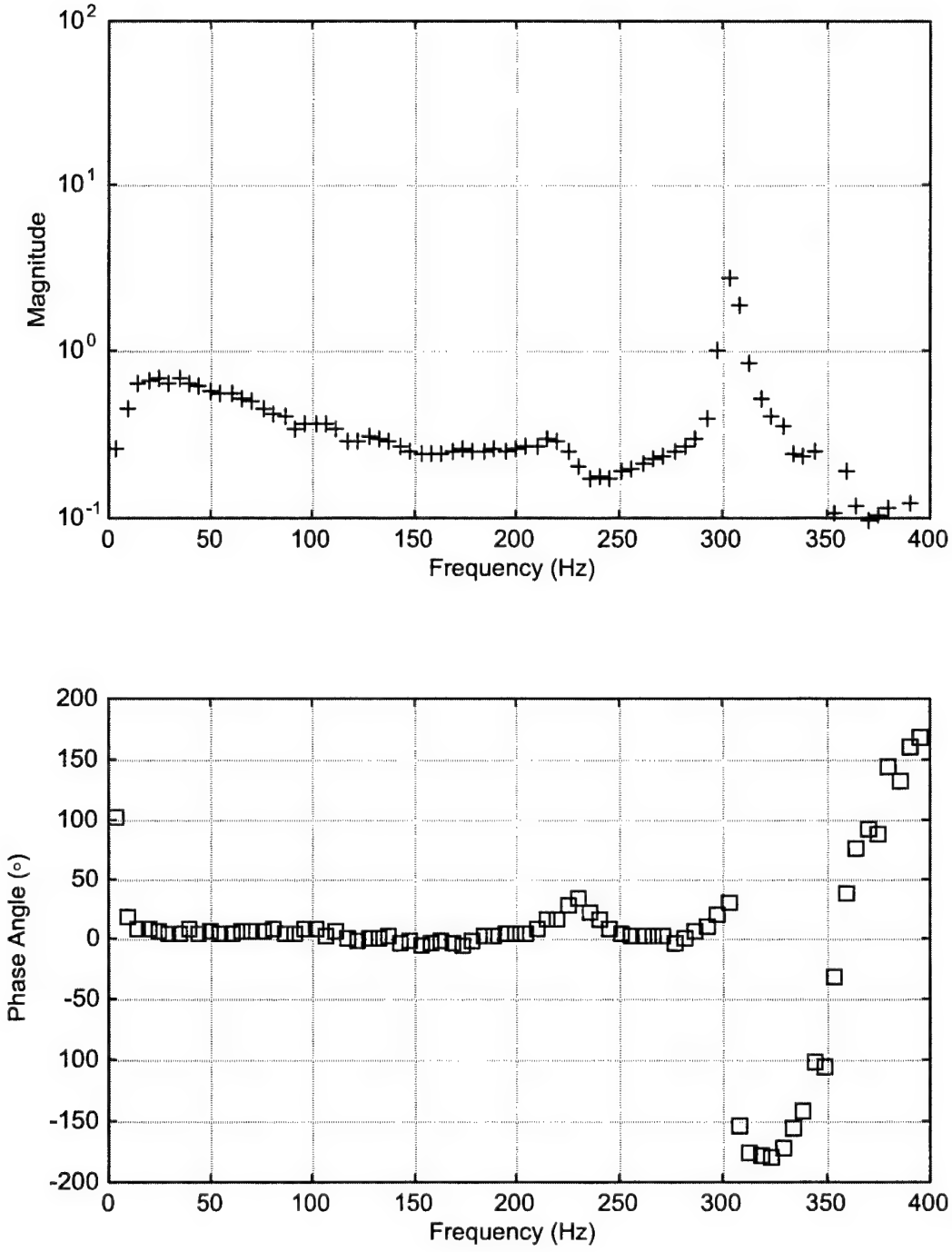

Figure 5. Estimation of Coefficient B Versus Frequency for Experiment

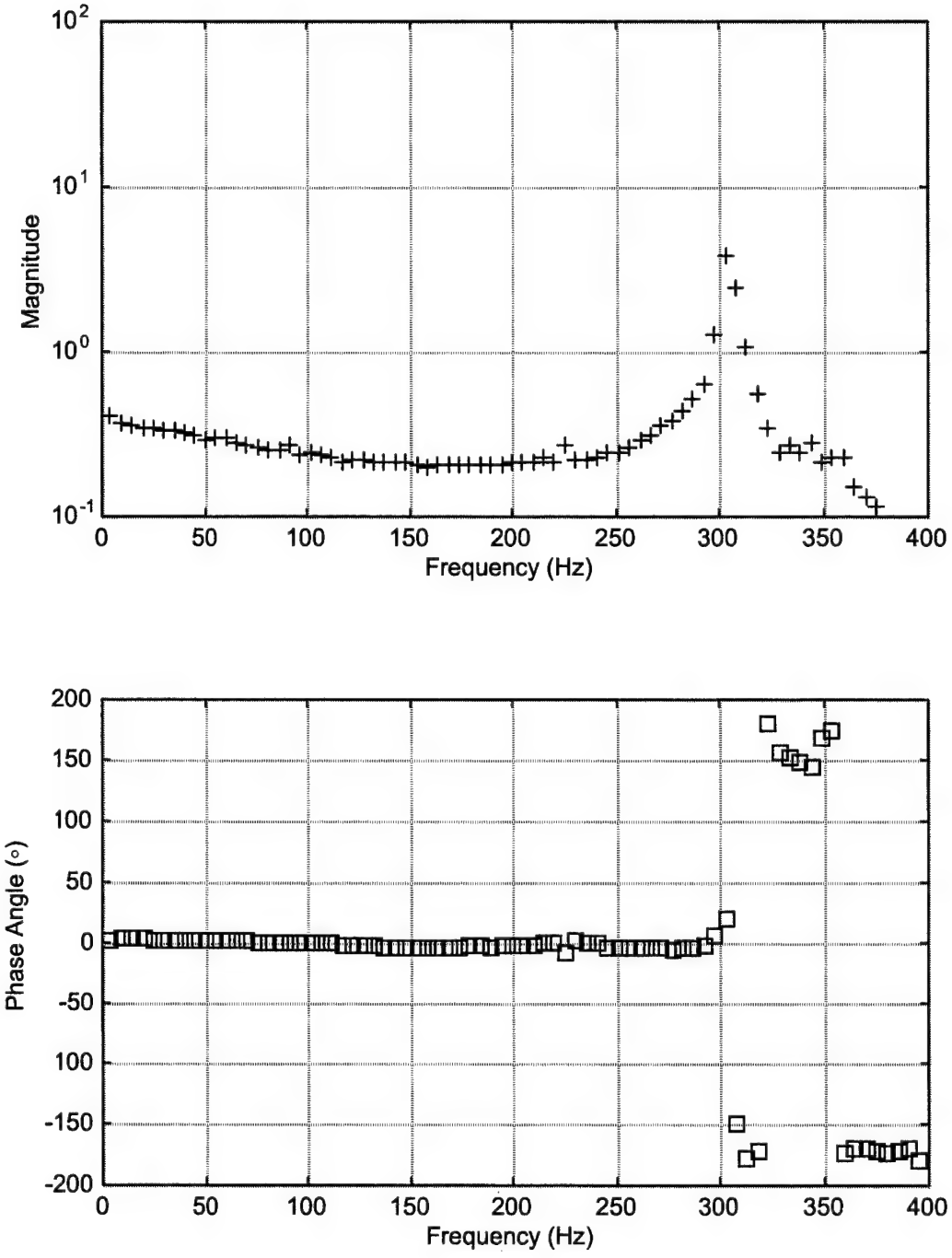

Figure 6. Estimation of Coefficient C Versus Frequency for Experiment

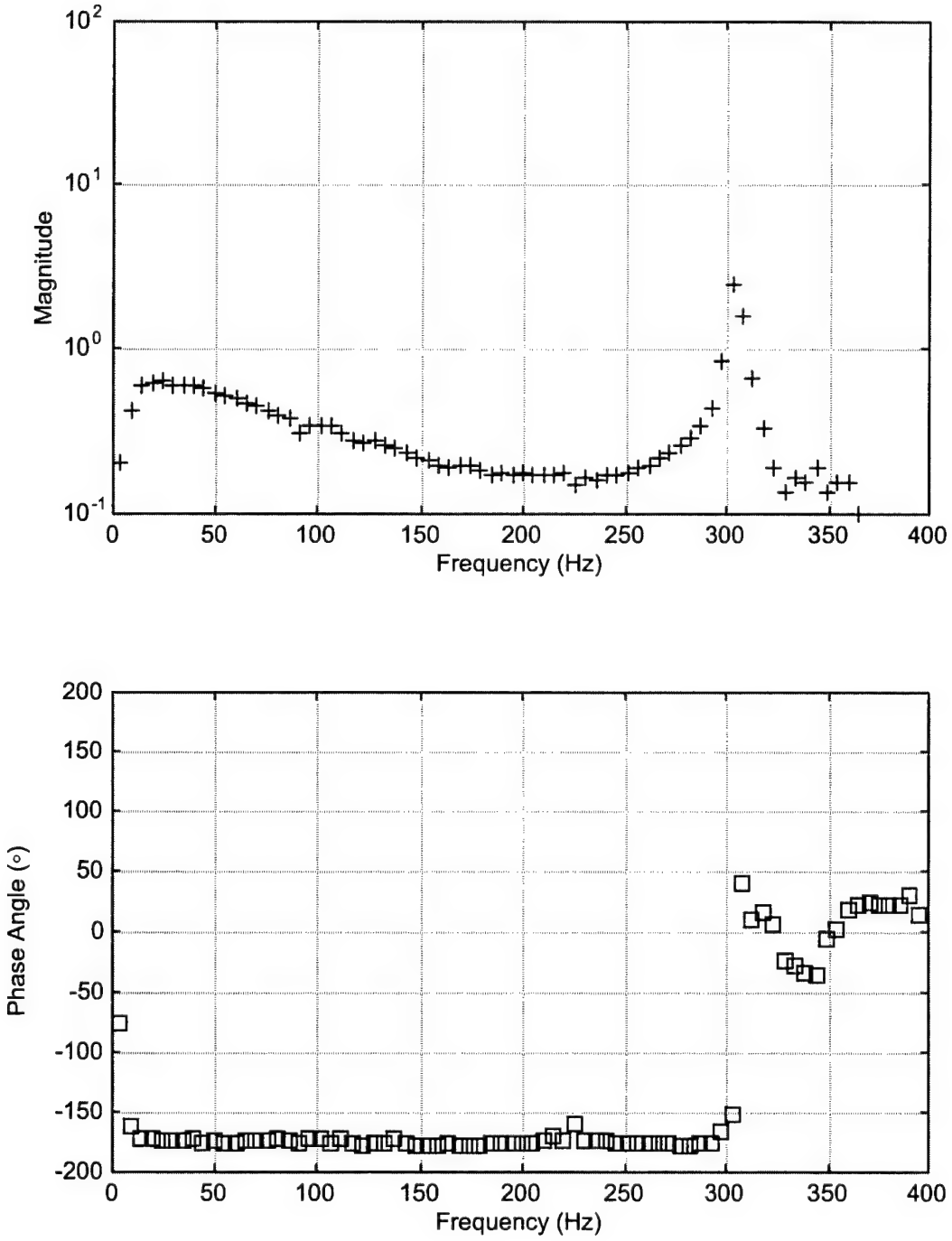

Figure 7. Estimation of Coefficient D Versus Frequency for Experiment

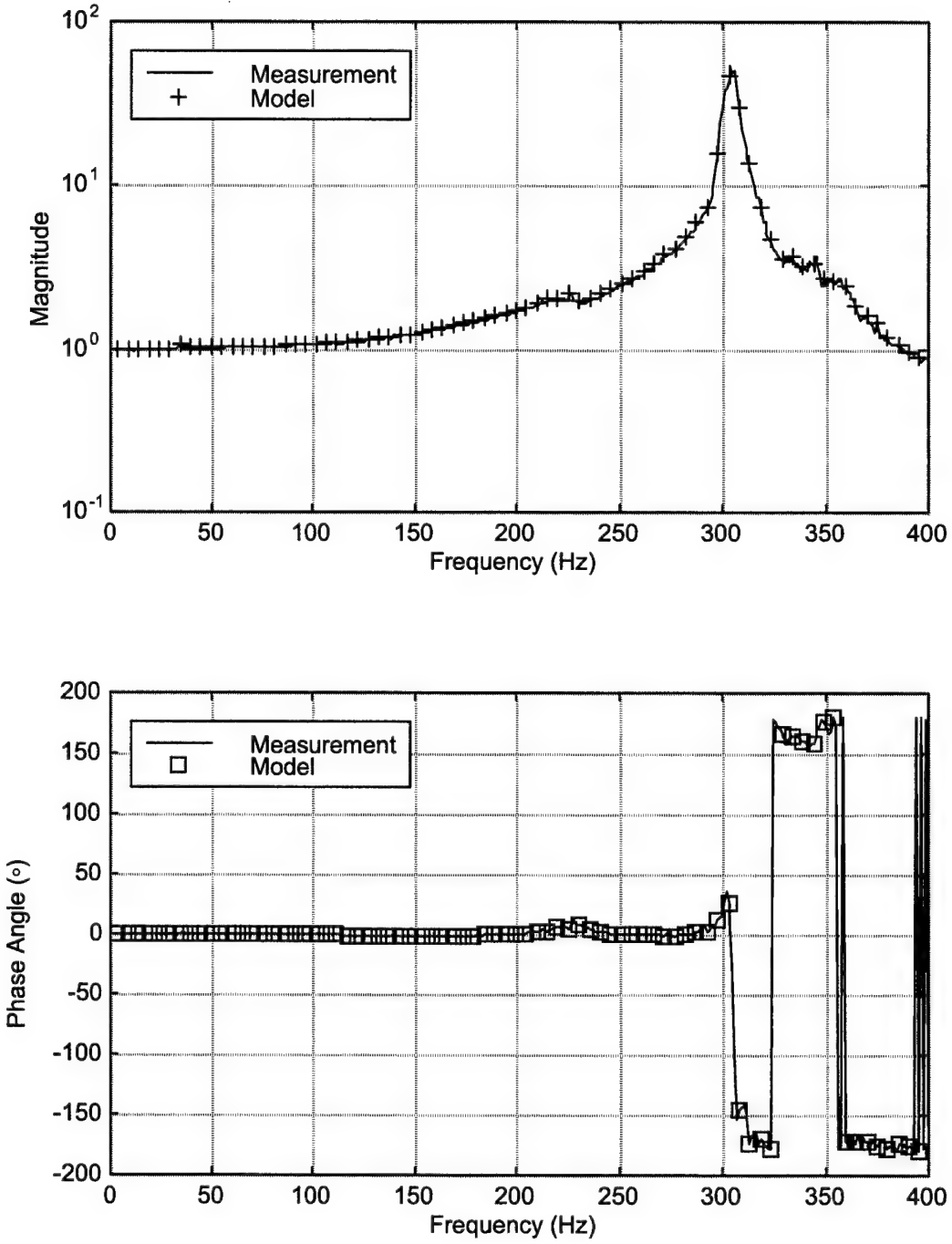

Figure 8. Measured and Estimated Transfer Function Versus Frequency

CONCLUSIONS

This report has derived an inverse method to measure the complex flexural wavenumber and wave propagation coefficients of a beam. The new approach obtains seven measured transfer functions by vibrating the beam transversely with any set of corresponding boundary conditions. These measurements are then combined to yield closed-form solutions of the beam parameters. Numerical simulations have shown that this approach is relatively immune to noise that has been added to the transfer function, and an experiment has validated the effectiveness of the technique when it is applied to laboratory data.

REFERENCES

1. R. de Prony, "Essai Experimental et Analytique," *Journal of Ec. Polytech*, Paris, France, vol. 1, 1795, pp. 24-76.

2. K. Grosh and E. G. Williams, "Complex Wave-Number Decomposition of Structural Vibrations," *Journal of the Acoustical Society of America*, vol. 93, no. 2, 1993, pp. 836-848.

3. Y. M. Ram, "Inverse Mode Problems for the Discrete Model of a Vibrating Beam," *Journal of Sound and Vibration*, vol. 169, no. 2, 1994, pp. 239-252.

4. J. Linjama and T. Lahti, "Measurement of Bending Wave Reflection and Impedance in a Beam by the Structural Intensity Technique," *Journal of Sound and Vibration*, vol. 161, no. 2, 1993, pp. 317-331.

5. P. D. Bauman, "Measurement of Structural Intensity: Analytic and Experimental Evaluation of Various Techniques for the Case of Flexural Waves in One-Dimensional Structures," *Journal of Sound and Vibration*, vol. 174, no. 5, 1994, pp. 677-694.

6. B. R. Mace and C. R. Halkyard, "Time Domain Estimation of Response and Intensity in Beams Using Wave Decomposition and Reconstruction," *Journal of Sound and Vibration*, vol. 230, no. 3, 2000, pp. 561-589.

7. L. L. Koss and D. Karczub, "Euler Beam Bending Wave Solution Predictions of Dynamic Strain Using Frequency Response Functions," *Journal of Sound and Vibration*, vol. 184, no. 2, 1995, pp. 229-244.

8. J. G. McDaniel, P. Dupont, and L. Salvino, "A Wave Approach to Estimating Frequency-Dependent Damping Under Transient Loading," *Journal of Sound and Vibration*, vol. 231, no. 2, 2000, pp. 433-449.

9. J. G. McDaniel and W. S. Shepard, Jr., "Estimation of Structural Wave Numbers from Spatially Sparse Response Measurements," *Journal of the Acoustical Society of America*, vol. 108, no. 4, 2000, pp. 1674-1682.

APPENDIX — CLOSED-FORM SOLUTION USED FOR THE NUMERICAL SIMULATIONS

The configuration used for the numerical simulations is a beam that has been mounted at each end to springs attached to a shaker table, as shown in figure A-1. With the middle of the beam used as the coordinate system origin, the shaker table generates a transverse structural input using boundary conditions that are modeled as

$$\frac{\partial^2 u(-L/2,t)}{\partial x^2} = 0 \ , \tag{A-1}$$

$$-EI\frac{\partial^3 u(-L/2,t)}{\partial x^3} = k_1[u(-L/2,t) - w(t)] \ , \tag{A-2}$$

$$\frac{\partial^2 u(L/2,t)}{\partial x^2} = 0 \ , \tag{A-3}$$

and

$$-EI\frac{\partial^3 u(L/2,t)}{\partial x^3} = k_2[u(L/2,t) - w(t)] \ , \tag{A-4}$$

where

$$w(t) = W_0(\omega)\exp(\mathrm{i}\omega t) \ . \tag{A-5}$$

Inserting equation (3) from the main text into equations (A-1), (A-2), (A-3), (A-4), and (A-5) yields the solution to the wave propagation coefficients. Inserting these solutions back into equation (3) gives the displacement of the system, which is sometimes called the forward solution. The wave coefficient A is

$$A = \frac{A_T}{A_B} \,, \tag{A-6}$$

where

$$\begin{aligned} A_T = {} & (k_1 - k_2)(EI\alpha^3)\cos\left(\alpha\frac{L}{2}\right)\cosh\left(\alpha\frac{L}{2}\right)\sinh\left(\alpha\frac{L}{2}\right) \\ & - (k_1 - k_2)(EI\alpha^3)\sin\left(\alpha\frac{L}{2}\right)\cosh^2\left(\alpha\frac{L}{2}\right) \\ & - (4k_1k_2)\sin\left(\alpha\frac{L}{2}\right)\cosh\left(\alpha\frac{L}{2}\right)\sinh\left(\alpha\frac{L}{2}\right) \end{aligned} \tag{A-7}$$

and

$$\begin{aligned} A_B = {} & 2(EI\alpha^3)^2\sin^2\left(\alpha\frac{L}{2}\right)\cosh^2\left(\alpha\frac{L}{2}\right) \\ & - 2(k_1 - k_2)(EI\alpha^3)\sin^2\left(\alpha\frac{L}{2}\right)\cosh\left(\alpha\frac{L}{2}\right)\sinh\left(\alpha\frac{L}{2}\right) \\ & - 2(EI\alpha^3)^2\cos^2\left(\alpha\frac{L}{2}\right)\sinh^2\left(\alpha\frac{L}{2}\right) \\ & - 2(k_1 - k_2)(EI\alpha^3)\cos\left(\alpha\frac{L}{2}\right)\sin\left(\alpha\frac{L}{2}\right)\sinh^2\left(\alpha\frac{L}{2}\right) \\ & + 2(k_1 - k_2)(EI\alpha^3)\cos^2\left(\alpha\frac{L}{2}\right)\cosh\left(\alpha\frac{L}{2}\right)\sinh\left(\alpha\frac{L}{2}\right) \\ & - 2(k_1 - k_2)(EI\alpha^3)\cos\left(\alpha\frac{L}{2}\right)\sin\left(\alpha\frac{L}{2}\right)\cosh^2\left(\alpha\frac{L}{2}\right) \\ & - 8(k_1k_2)\cos\left(\alpha\frac{L}{2}\right)\sin\left(\alpha\frac{L}{2}\right)\cosh\left(\alpha\frac{L}{2}\right)\sinh\left(\alpha\frac{L}{2}\right) \,. \end{aligned} \tag{A-8}$$

The wave coefficient B is

$$B = \frac{B_T}{B_B} \,, \tag{A-9}$$

where

$$B_T = -(k_1 + k_2)(EI\alpha^3)\sin\left(\alpha\frac{L}{2}\right)\cosh\left(\alpha\frac{L}{2}\right)\sinh\left(\alpha\frac{L}{2}\right)$$
$$- (k_1 + k_2)(EI\alpha^3)\cos\left(\alpha\frac{L}{2}\right)\sinh^2\left(\alpha\frac{L}{2}\right) \tag{A-10}$$

and

$$B_B = 2(EI\alpha^3)^2\cos^2\left(\alpha\frac{L}{2}\right)\sinh^2\left(\alpha\frac{L}{2}\right)$$
$$- 2(k_1 - k_2)(EI\alpha^3)\cos^2\left(\alpha\frac{L}{2}\right)\cosh\left(\alpha\frac{L}{2}\right)\sinh\left(\alpha\frac{L}{2}\right)$$
$$- 2(EI\alpha^3)^2\sin^2\left(\alpha\frac{L}{2}\right)\cosh^2\left(\alpha\frac{L}{2}\right)$$
$$+ 2(k_1 - k_2)(EI\alpha^3)\cos\left(\alpha\frac{L}{2}\right)\sin\left(\alpha\frac{L}{2}\right)\cosh^2\left(\alpha\frac{L}{2}\right)$$
$$+ 2(k_1 - k_2)(EI\alpha^3)\sin^2\left(\alpha\frac{L}{2}\right)\cosh\left(\alpha\frac{L}{2}\right)\sinh\left(\alpha\frac{L}{2}\right)$$
$$+ 2(k_1 - k_2)(EI\alpha^3)\cos\left(\alpha\frac{L}{2}\right)\sin\left(\alpha\frac{L}{2}\right)\sinh^2\left(\alpha\frac{L}{2}\right)$$
$$+ 8(k_1 k_2)\cos\left(\alpha\frac{L}{2}\right)\sin\left(\alpha\frac{L}{2}\right)\cosh\left(\alpha\frac{L}{2}\right)\sinh\left(\alpha\frac{L}{2}\right) . \tag{A-11}$$

The wave coefficient C is

$$C = \frac{C_T}{A_B} , \tag{A-12}$$

where

$$C_T = (k_1 - k_2)(EI\alpha^3)\cos^2\left(\alpha\frac{L}{2}\right)\sinh\left(\alpha\frac{L}{2}\right)$$
$$- (k_1 - k_2)(EI\alpha^3)\cos\left(\alpha\frac{L}{2}\right)\sin\left(\alpha\frac{L}{2}\right)\cosh\left(\alpha\frac{L}{2}\right)$$
$$- 4(k_1 k_2)\cos\left(\alpha\frac{L}{2}\right)\sin\left(\alpha\frac{L}{2}\right)\sinh\left(\alpha\frac{L}{2}\right) . \tag{A-13}$$

The wave coefficient D is

$$D = \frac{D_T}{B_B} , \tag{A-14}$$

where

$$D_T = -(k_1 + k_2)(EI\alpha^3)\sin^2\left(\alpha\frac{L}{2}\right)\cosh\left(\alpha\frac{L}{2}\right) - (k_1 + k_2)(EI\alpha^3)\cos\left(\alpha\frac{L}{2}\right)\sin\left(\alpha\frac{L}{2}\right)\sinh\left(\alpha\frac{L}{2}\right) . \tag{A-15}$$

These coefficients are used for the numerical simulations in the main text.

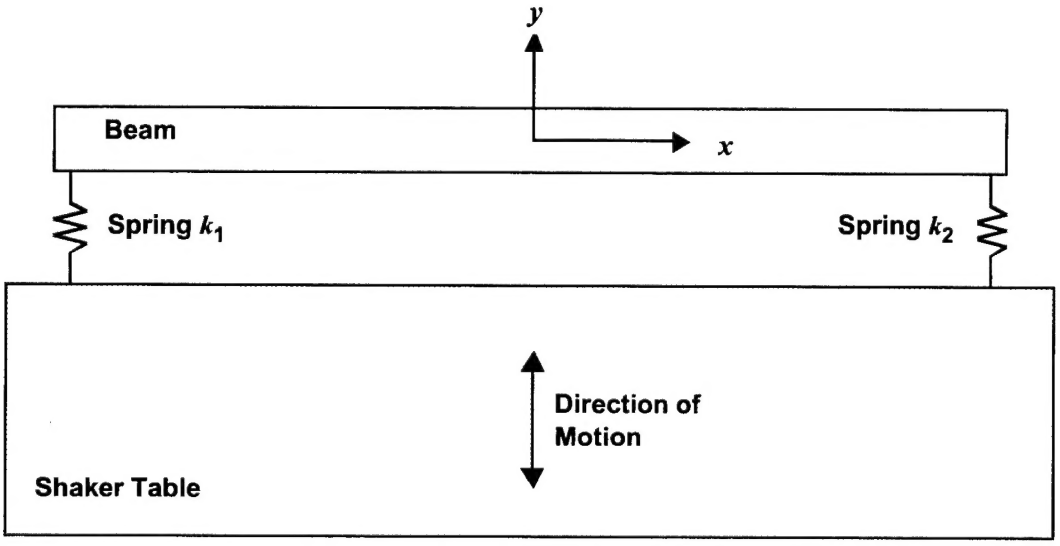

Figure A-1. Beam with Two Springs Attached to the Shaker Table

INITIAL DISTRIBUTION LIST

Addressee	No. of Copies
Office of Naval Intelligence (ONI 241 – J. Pickering, J. Zilius, T. Morgan)	3
Office of Naval Research (ONR 321 – D. Davidson, R. Elswick; ONR 313 – D. McGregor)	3
Defense Technical Information Center	2
Center for Naval Analyses	1